J Mater Sci (2009) 44:5274–5287
DOI 10.1007/s10853-009-3664-8

FERROELECTRICS

Interface effects on highly epitaxial ferroelectric thin films

Y. Lin · C. L. Chen

Received: 8 April 2009 / Accepted: 3 June 2009 / Published online: 23 June 2009

Abstract Interface effects have been found to play a key role in controlling the epitaxial nature and physical properties on the highly epitaxial ferroelectric thin films. Thin film ferroelectrics are dominantly affected by the strains induced by lattice misfits between the films and the substrates, surface step terrace, both step height and terrace dimension, and the surface terminations. The natures of interface induced local strain formations, edge dislocations, and antiphase domain boundaries are reviewed in this article.

Introduction

Ferroelectric materials, such as $Ba_{1-x}Sr_xTiO_3$ (BST-x), $Pb_{1-x}Sr_xTiO_3$ (PST-x), etc., with nonlinear dielectric properties have been recognized for their importance as extraordinary functional materials due to their attractive dielectric properties, such as high dielectric constant, low dielectric loss, spontaneous polarization, and strong field dependence of dielectric constant. Notably, the field dependence of the dielectric constant results in a tunable dielectric response through the application of an external electrical field. A great effort has been made in the past two decades towards applying these nonlinear dielectric properties, found in highly epitaxial thin films, to applications in tunable microwave devices, structural health monitoring systems, nonvolatile memories and memory capacitors, and many other microelectronic and electro-optic devices [1–5].

However, it has been found that the dielectric properties of these ferroelectric thin films are quite different from those of their bulk [6]. The strong dependence of the dielectric properties on various substrates has been observed [7–12]. On the other hand, the ferroelectricity is seriously affected by the film thickness [13–27]: (1) Normally, the dielectric constant and remanent polarization change markedly with the decrease of film thickness when the films are thinner than the critical thickness; (2) a significant broadening of the peak of the dielectric constant as a function of the temperature occurs in thinner films. These results imply that the interfaces have played a key role in the dielectric properties of highly epitaxial ferroelectric thin films. In particular, when the thickness of the films scaled down to nanometers, or the ratio of interface to bulk material is comparable, the interface contribution to the properties of these films/heterostructures becomes dominant.

When a film is grown on a substrate, an interface is formed between the film and the substrate surface. Normally, the film is grown in a way with minimum interface energy. Important factors that affect the interface include the crystal structures, surface and interfacial energies, bonding configurations, and the thermal expansion coefficient of the film and the substrate, etc. Many efforts have been made to explore interfacial behavior and its effect on the properties of thin films.

In this article, we will focus on the discussion of the effect from the strain, dislocations and antiphase domain boundaries near/at the interface in highly epitaxial ferroelectric thin films and multilayered structures.

Y. Lin
State Key Laboratory of Electronic Thin Films and Integrated Devices, University of Electronic Science & Technology of China, Chengdu, Sichuan 610054, People's Republic of China

C. L. Chen (✉)
Department of Physics and Astronomy, University of Texas at San Antonio, San Antonio, TX 78249, USA
e-mail: cl.chen@utsa.edu

Strain-induced edge dislocation formations

When a thin ferroelectric layer grows on a substrate, especially in the partially coherent growth mode, stress can be generated from the lattice misfit, thermal mismatch and phase transformations between the substrate and the film. As mentioned above, this stress may lead to the strain in the film and drastically influence the film growth mode, the microstructures in the films, and the physical properties. It may change the film surface morphologies, induce dislocations and defects in the films, and result in a variety of interesting and anomalous new physical phenomena.

Strain effects on ferroelectric properties have been theoretically studied from Devonshire thermodynamic formalism as early as 1949, which revealed that the Curie temperature will be changed under a two-dimensional stress [28, 29]. At the end of the 1980s, Cross and his collaborators theoretically calculated the coefficients of a modified Devonshire energy function for $PbTiO_3$ and successfully predicted the shift of the Curie point with hydrostatic stress [30, 31]. Using the thermodynamic theory, along with the X-ray results, they plausibly explained the shift of the Curie point in *c*-axis oriented $PbTiO_3$ thin films, observed by Kushida et al. [32, 33], in terms of a two-dimensional stress effect [34]. Lately, Pertsev et al. [35, 36] further developed the Landau–Devonshire thermodynamic model for epitaxial ferroelectric films and predicted the appearance of unusual phases and phase transformations as a result of the epitaxy induced internal stresses. The strain–temperature phase diagrams were successfully developed for epitaxial $BaTiO_3$ and $PbTiO_3$ films, and were experimentally confirmed by Streiffer et al. [37], when it was found that the reduction in the apparent Curie–Weiss temperature, observed in fiber-textured BST-*x* thin films on Si substrates, was due to the tensile stress.

The generation of dislocations has been widely accepted as a major mechanism to release this induced strain. Typically, edge dislocations can be formed at or near the interface to fully or partially release interface strain energy due to lattice misfit between the film and the substrate, as seen in Fig. 1. The recent experimental observations, from the high-resolution electron microscope by Chen et al. [38], reveal that the edge dislocations are uniformly formed along the entire interfaces of the ferroelectric BST-0.5 on (001) $LaAlO_3$, as seen in Fig. 2. The formation of misfit dislocations during deposition can reduce the strain energy accumulated in the films and alter the energy distribution functions. By considering the misfit dislocations formed at the interface during the film growth, Ban and Alpay [39] theoretically investigated single-domain epitaxial BST-*x* films on a series of cubic substrates based on the cube-on-cube epitaxy and also developed phase diagrams of these systems as a function of the misfit strain based on a Landau–Devonshire phenomenological model. This model is a new version of the Pertsev's model and becomes a milestone in understanding the strain effects on oxide thin film growth. It is clearly shown that the dielectric response is strongly dependent upon the film thickness and the misfit strain via substrate selection, especially in the vicinity of structural instabilities, which sheds light on the strain

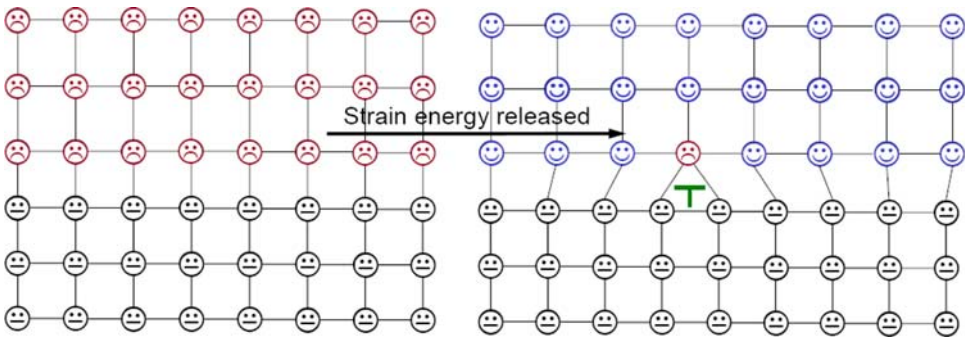

Fig. 1 Schematic illustration of the mechanisms of edge dislocation formed at the interface to reduce the strain energy in the highly epitaxial films [12]

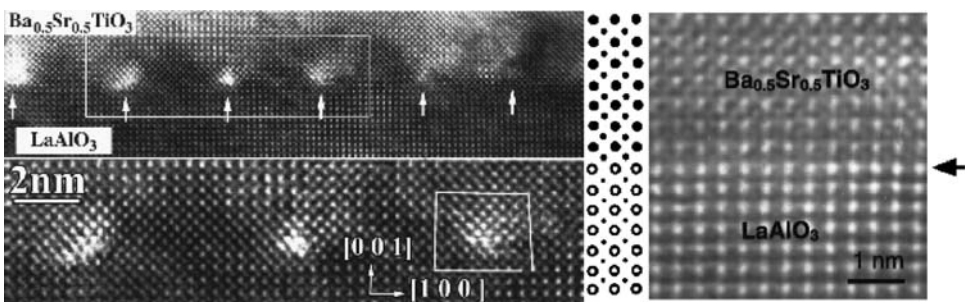

Fig. 2 High-resolution TEM image of $Ba_{0.5}Sr_{0.5}TiO_3$/LaAlO3 showing the edge dislocations were uniformly distributed along the entire interface [38]

engineering of ferroelectric thin films. Detailed theoretical analysis can be found in the recent literature [40] or the recent review article by Alpay in this special issue.

Experimentally, lattice misfit dislocations, normally in the form of edge dislocations, can be directly observed from cross-sectional Transmission Electron Microscopy (TEM) with the image of the crystal structure of thin films perpendicular to the film surface [41]. Figure 3a is a bright field cross-sectional TEM image of an epitaxial ferroelectric PST-0.4 (PSTO) thin films on (001) MgO. The selected-area electron diffraction (SAED) were taken with the electron beam parallel to the [100] axis of MgO. Figure 3b, c, and d are SAED patterns taken from the film, the area covering both the film and the substrate, and the substrate, respectively, showing a single cubic crystal structure with excellent single crystallinity and a sharp interface. The interface relationship between the PSTO film and the MgO substrate is determined to be $(001)_{PSTO}//(001)_{MgO}$ and $\langle 100\rangle_{PSTO}//\langle 100\rangle_{MgO}$ and the lattice mismatch can be estimated as -6.2% calculated using $(\boldsymbol{a}_{PSTO}-\boldsymbol{a}_{MgO})/\boldsymbol{a}_{MgO}$ measured from the electron diffraction pattern. The high-resolution TEM image of the interface taken under two-beam condition, as shown in Fig. 3e, reveals the periodically distributed edge dislocations at the interface accommodated the lattice misfit strain with the average spacing of the edge dislocations of about 2.8 nm.

These edge dislocation networks and strain distributions can also be seen clearly from plan-view images in which an image is along the surface plane of the film. The interface structures of the PST-0.4 (PSTO) thin film on (001) MgO substrate was also studied by using the double diffraction technique of a plan-view High-resolution TEM (HRTEM) [42]. As seen in Fig. 4a, groups of diffraction spots in a SAED pattern of the interface taken from a plan-view PSTO/MgO sample with the electron beam entering the PSTO film and exiting from the MgO substrate. This SAED pattern exhibits quite different characteristics from those shown in Fig. 3b, i.e., it cannot be obtained by simply superimposing the diffraction patterns of PSTO [001] zone and MgO [001] zone. A modulated structure was clearly observed from this plan-view PSTO/MgO sample. The modulation wavelength measured from Fig. 4b is about 2.7 nm, which is very close to the value obtained from the SAED pattern in Fig. 4a. Figure 4d is a Fourier transformation (FT) of the HRTEM image in Fig. 4c presenting a diffraction pattern similar to the SAED in Fig. 4a. Figure 4a shows many more diffraction spots compared to Fig. 3b and presents a complicated pattern similar to those observed in some incommensurate or commensurate modulated structures. Figure 4a exhibits a fourfold symmetry. All of the diffraction spots including strong and weak ones are located in a two-dimensional square superlattice with a lattice constant of 2.73 nm. This value equals to either 14 times the *d*-spacing of PSTO (200), or 13 times the *d*-spacing of MgO (200).

PSTO has a cubic perovskite structure with (Pb, Sr) atoms distributed at (000), Ti at (½ ½ ½) and O at (½ ½ 0), (0 ½ ½), and (½ 0 ½) positions. MgO is a rock-salt type structure with Mg atoms occupying (000), (½ ½ 0), (0 ½ ½), and (½ 0 ½), and O occupying (½ 0 0), (0 ½ 0), (0 0 ½), and (½ ½ ½) positions. Diffraction spots in Fig. 4b can be obtained using double diffraction of the MgO [001] and PSTO [001] zone diffraction patterns. Figure 4c shows a schematic classification of the diffraction spots in a quarter of the SAED pattern of Fig. 4a, where open circles, dark, and gray spots represent the diffraction spots from MgO, PSTO, and double diffractions, respectively. The reciprocal lattice vector $g_{hkuv}$of a diffraction spot in Fig. 4a can be given by

$$g_{hkmn} = ha^*_{MgO} + ua^*_{PSTO} + kb^*_{MgO} + vb^*_{PSTO},$$

where *h, k, u*, and *v* are all integers, a^*_{MgO} and b^*_{MgO} are unit vectors of MgO in reciprocal space, a^*_{PSTO} and b^*_{PSTO} correspond to the reciprocal unit vectors of PSTO. The diffraction spots in Fig. 4a can then be indexed using four indices (*h k u v*). For example, diffraction spots 1, 2, 3, 4, 5,

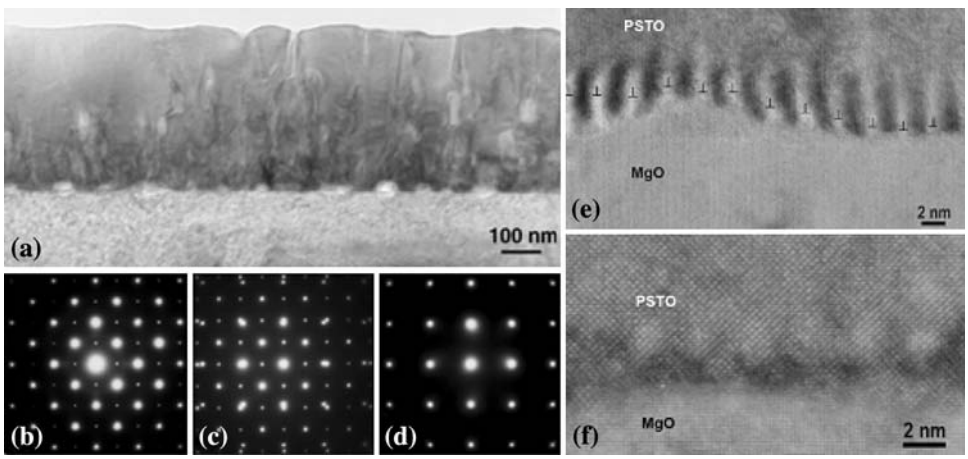

Fig. 3 *Left* **a** Cross-sectional TEM image of PSTO/MgO, **b–d** SAED from PSTO film, interface covering both PSTO and MgO, and MgO substrate, respectively. *Right* **e** Two-beam and **f** multi-beam cross-section HRTEM image of the PSTO/MgO interface [41]

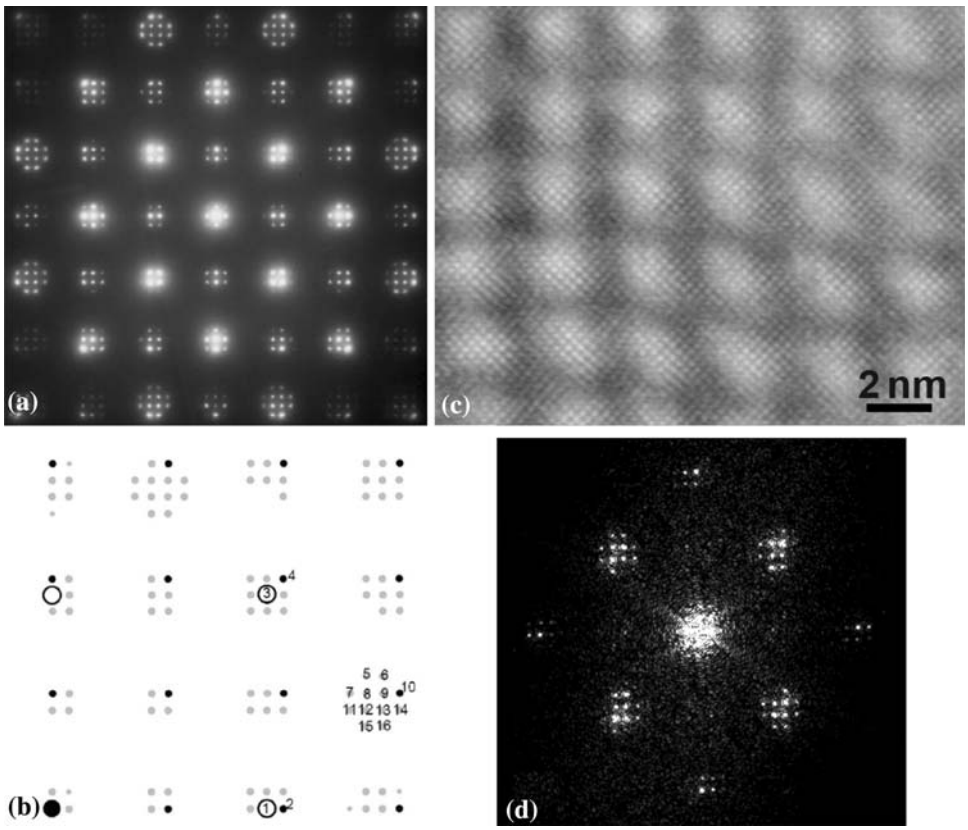

Fig. 4 **a** SAED pattern of the plan-view PSTO/MgO interface, **b** schematic illustration showing classification of the diffraction spots. *Open circles* MgO; *dark spots* PSTO; *gray spots* double diffractions. **c** Plan-view HRTEM image of the PSTO/MgO interface, **d** Fourier transformation of **a** [41]

and 6 in Fig. 4c can be indexed using (2 0 0 0), (0 0 2 0), (2 2 0 0), (0 0 2 2), (4 $\bar{2}$ $\bar{1}$ 3) and (2 $\bar{2}$ 1 3), respectively. The indices of the marked diffraction spots in Fig. 4c are summarized in Table 1. Diffraction spots with (*h k* 0 0) indices correspond to the MgO, while those with (0 0 *u v*) correspond to the PSTO. The diffraction spots with (*h k u v*) (*h, k, u,* and *v* are non-zero integers) correspond to the double diffraction spots.

The uniform distribution of edge dislocation network in the as-grown PST-0.4 films suggests that the formation of edge dislocations at the interface between the film and substrate can significantly reduce the interface strain energy, most probably from the lattice misfit. Such an interface structure will also alter the physical properties of the highly epitaxial thin films. The effects on the physical properties of the highly epitaxial ferroelectric PST thin films can be understood by the models in the previous theoretical [43–45] and experimental studies [46–51].

Table 1 Indices (*h k u v*) of the marked diffraction spots in Fig. 4c

Number	Indices	Number	Indices
1	(2 0 0 0)	9	(2 0 1 1)
2	(0 0 2 0)	10	(0 0 3 1)
3	(2 2 0 0)	11	(6 2 $\bar{3}$ $\bar{1}$)
4	(0 0 2 2)	12	(4 2 $\bar{1}$ $\bar{1}$)
5	(4 $\bar{2}$ $\bar{1}$ 3)	13	(2 2 1 $\bar{1}$)
6	(2 $\bar{2}$ 1 3)	14	(0 2 3 $\bar{1}$)
7	(6 0 $\bar{3}$ 1)	15	(4 4 $\bar{1}$ $\bar{3}$)
8	(4 0 $\bar{1}$ 1)	16	(2 4 1 $\bar{3}$)

The physical nature of the dislocations effect has been investigated by a couple of groups [52–56]. Based on the thermodynamic model, polarization distribution is spatially non-uniform near the dislocation due to the coupling of the stress field and the polarization. The polarization gradients result in strong depolarizing fields that suppress the polarization in a region that extends over several nanometers. The applied electrical field that is necessary to activate the unique properties of ferroelectrics will essentially be screened. On the other hand, these regions may serve as pinning centers for reversible 180° and non-180° domain wall motion in the presence of an applied field [52, 53]. Local charges accumulated on interfacial dislocations and some other grain boundaries have also been considered as factors that degrade the dielectric and ferroelectric properties [54]. However, in a recent theoretical work performed by Li et al. [55], it was found that the hysteresis loop is dependent not only density but also the type of interfacial dislocations. The influence of interfacial dislocations on the ferroelectric properties was studied using phase-field simulations. For $BaTiO_3$ epitaxial thin films, it was found that an optimal combination of misfit dislocations with certain burgers vectors can produce a relatively

smaller coercive field but larger remanent polarization. This finding points to a new route to the strain engineering of the properties of ferroelectric thin films.

Surface step terrace dimensions induced local strain formation

The early discussion has demonstrated that the lattice misfit induced strain energy in the hetero-epitaxial system can be partially or fully released at the interface between epitaxial films and substrates via formation of edge dislocations that periodically distribute along the interface. However, even films grown under optimal conditions, as discussed previously, can not achieve optimum ferroelectric properties, as the lattice matching and surface-step-terrace structure can alter the film microstructure, which may result from the substrate surface structures, i.e., substrate surface terminations, surface terrace dimensions, step heights, and other surface defects. Neither experimental nor theoretical research has been conducted to systematically investigate the effect of the mismatch between the film unit-cell arrangement and the substrate surface-step-terrace dimensions, named as "residual matching". It should be noted that there are a large number of surface-step-terraces on single crystal surfaces [57]. Normally, a surface-step-terrace will not match an exact number of unit cells or atomic planes in the film, as seen in the Fig. 5. The mismatch of film unit cells/substrate terrace, residual matching, will result in an additional strain energy that can not be released via edge dislocations and will be stored in the hetero-epitaxial films. As the film continues to grow away from the surface, the residual matching-induced strain energy will accumulate in the hetero-epitaxial film and can significantly alter its microstructure and thus, its physical and electrical properties. In fact, the effect of surface-step-terrace on the epitaxial nature of highly epitaxial oxide thin films can be considered in two factors: step height and terrace dimension. The step height can result in the formation of anti-phase domain boundaries, both conservative and non-conservative boundaries. The terrace dimension effect is normally neglected in thin film growth. Unlike metal or semiconductor thin films, ionic thin film growth requires a good match in the combination of positive and negative charge balance. Theoretically, when a number of film unit cells fill up along the terrace, a mismatch gap can be generated at the end of the step terrace, which is the "residual matching". Practically, this mismatch gap will not exist at the end of step terrace in an epitaxial film. The last atomic plane of the film will always occupy the atomic position of the terrace end via a rearrangement of the local atomic structure. Thus, the atomic position change can significantly increase the growth potential and alter the epitaxial quality.

Recently, Chen and his collaborators [58, 59] have systematically investigated the effect of the residual matching generated from the mismatch between the film unit cells and terrace dimension. Different vicinal surfaces were created from various miscut (001) MgO substrates to epitaxially grow the ferroelectric BST-0.4 thin films. The various miscut (001) MgO substrates can provide different surface-step-terrace dimensions on the vicinal surfaces.

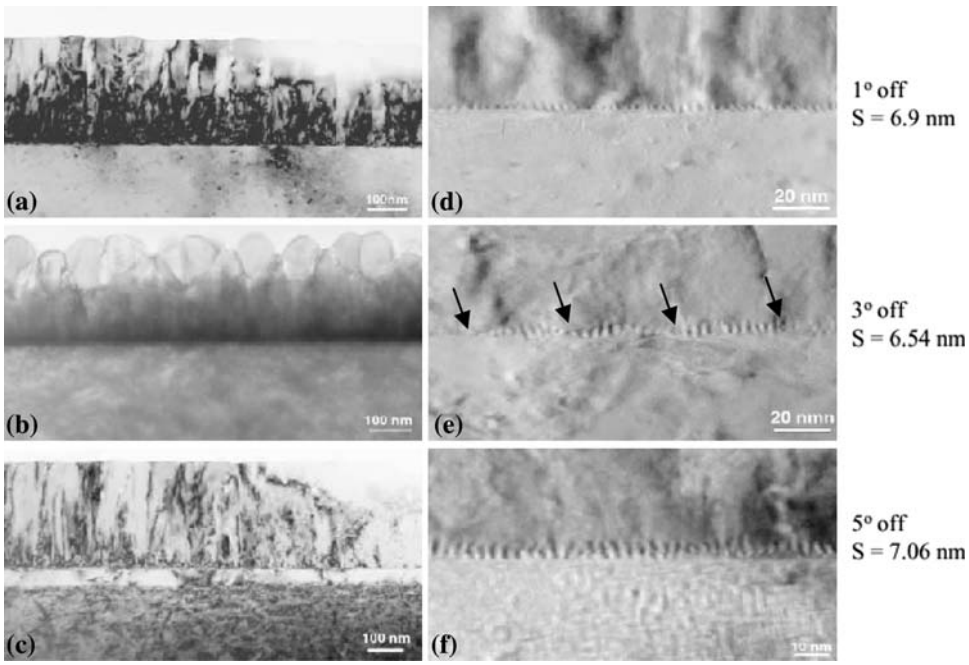

Fig. 5 **a–c** are cross-sectional TEM images showing the epitaxial behavior and **d–f** are the interface structures for the BSTO films grown on 1°, 3°, and 5° miscut substrate surfaces, respectively. **d–f** Edge dislocation distributions for the BSTO films grown on 1°, 3°, and 5° the interface are periodic (**d**, **f**) and quasi-periodically (**e**) distribution [59]

With miscut angles of 1°, 3°, and 5° on the (001) vicinal MgO surfaces, the average step terrace dimension can be simply estimated to be 12.0, 4.02, and 2.40 nm, respectively. These dimensions are corresponding to the average BSTO unit cells of 30.5, 10.2, and 6.04 on the 1°, 3°, and 5° vicinal surface terraces. The dielectric property measurements from the epitaxial Mn-doped (2% Mn extra doping) BST-0.4 (Mn:BSTO) films grown on these miscut (001) MgO vicinal surfaces have shown that the dielectric constant and dielectric tunability of films grown on 1° and 5° miscut (001) MgO surfaces have very similar properties with the normal (0° miscut) substrates. However, both the dielectric constant and dielectric loss for the film grown on 3° miscut substrate are two-thirds of that for the films grown on 1° and 5° miscut (001) MgO surfaces. This dramatic difference in dielectric properties is due to the mismatch between the film unit cells in-plane and the terrace dimensions.

Cross-sectional TEM was employed to study and understand the epitaxial quality and interface structures of the BST-0.4 films and the (001) MgO vicinal substrates. Figure 5a–c are X-TEM images showing the epitaxial behavior and d–f are the interface structures for the BSTO films grown on 1°, 3°, and 5° miscut substrate surfaces, respectively. The insets in Fig. 5a–c are the selected area electron diffraction patterns (SAED) taken along the [100] zone of the MgO lattice. The SAED patterns indicate that all of the films deposited on the miscut vicinal surfaces have good single crystallinity. The films grown on 1° and 5° miscut substrates reveal excellent hetero-epitaxy with very smooth surfaces and very sharp interfaces. Furthermore, edge dislocations are uniformly distributed along their entire interfaces. However, the film grown on the 3° miscut (001) MgO substrate is very different. It is observed that the film consists of two layers: a highly epitaxial layer on the miscut MgO substrate and a top polycrystalline-like layer. However, the electron diffraction pattern (inset in Fig. 5b), clearly shows that all of the particle-like grains are well aligned along the *c*-axis. Although the interface between the epitaxial film and the MgO substrate is very sharp, the film surface is rough (as high as 50 nm). Also, rather than the uniform dissemination, the edge dislocations along the interface are quasi-periodically distributed with a period close to 4.0 nm, as marked by arrows in Fig. 5e. These phenomena can be understood by considering the unit-cell arrangement on the substrate terraces.

As seen in Fig. 6a, the film unit cells are orderly aligned on each terrace of the (001) MgO substrate surface. The surface terminations on the (001) MgO surface are always the MgO layer although each neighboring MgO layer has half unit-cell height difference. Previous studies of BSTO films on (001) MgO have indicated that the TiO_2 layer is the

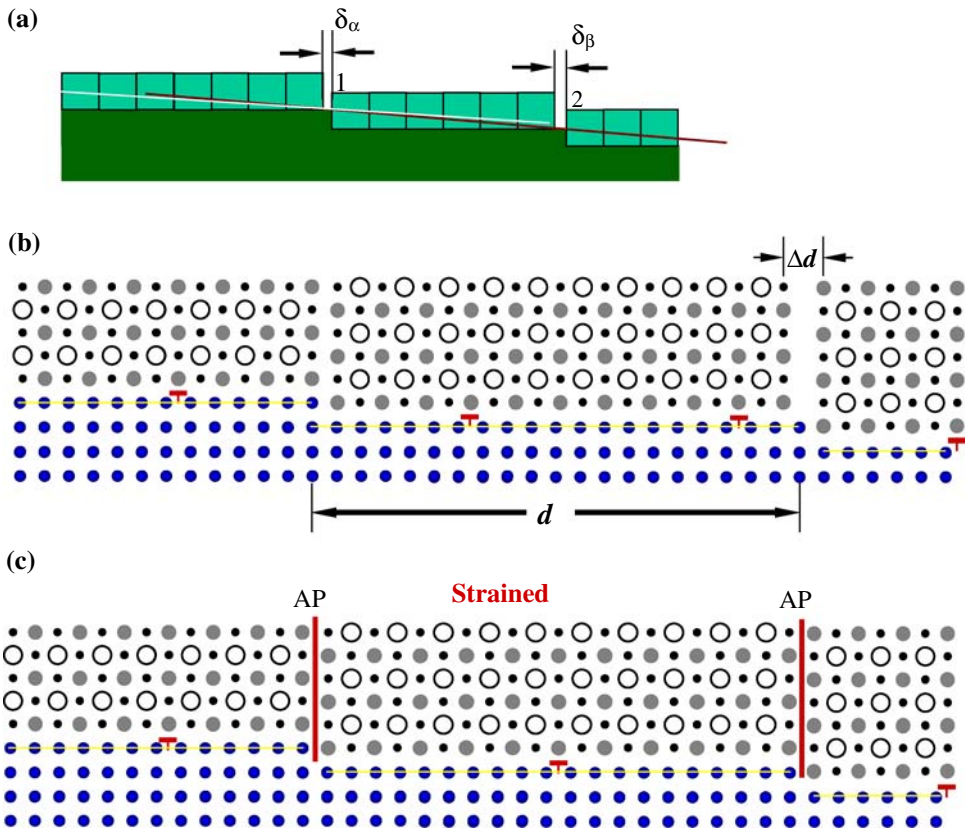

Fig. 6 Schematic illustration showing the surface-step-terrace dimension is normally not match an exact number of unit cells or atomic planes in the film. This mismatch of film unit cells/substrate terrace will result in strong strain energy that cannot be released via edge dislocations and will be stored in the hetero-epitaxial films [59]

nucleation layer of the film [47]. Thus, when BSTO grows on the (001) MgO substrate, the hetero-epitaxial BSTO film on each terrace becomes a single domain and the film consists of many domains which are shifted half unit cell along the *c*-axis if the neighbor terraces are single-step height terraces. The antidomain boundaries are therefore formed at the end of each step terrace. Details can be found in the literature [12]. When the BSTO unit cells orderly align along a terrace, the number of BSTO unit cells is determined by the dimension of the terrace. It should be noted that the dimensions of a terrace are not equal to an exact numbers of BSTO unit cells. Theoretically, the difference of the match between the BSTO unit cells and terrace dimensions will generate a small space gap Δd on each terrace, as seen in Fig. 6b. However, because of the lattice misfit and the unit-cell mismatch on the terrace, each terrace end in the epitaxial growth is always the atomic plane of the film, which results in the unit cells being rearranged on the terrace, as shown in Fig. 6c. This rearrangement results in the formation of local strain domain. The mismatch strain is completely depended upon the mismatch of the film unit cells and terrace dimension d, or simply, the size of the mismatch gap Δd. The lattice mismatch induced strain can be defined as $\delta = \Delta d/d$. Unlike the lattice misfit in the film growth, the mismatch-induced strain cannot be released via formation of edge dislocations that generally occur in the lattice misfit. This situation was examined in the ferroelectric thin films on various vicinal MgO substrate surfaces.

For the films grown on vicinal (001) MgO surfaces, the mismatch gaps can be estimated to be 0.0, 0.2, and 0.04 unit cells for the miscut of 1°, 3°, and 5°, respectively. These produce the average local strain levels in the highly epitaxial BSTO films of 0.000, 0.020, and 0.007, respectively. Thus, the films on 1° and 5° miscut substrates have much strain that the film on the 3° miscut substrate. Especially, the strain on the 3° miscut terrace is more than 3 times larger than that on the 5° miscut surfaces. With film growth, the strain energy will be rapidly accumulated and stored in the films and a large strain ultimately alters the epitaxial behavior by forming the polycrystalline-like particles once the film is thicker than a critical thickness. This phenomenon is evident in the X-TEM image in the Fig. 5b and can be well-understood by growth dynamics under strain.

Surface step terrace induced antiphase domain boundary formations

On the other hand, the surface step height and surface terminations have also played key roles in affecting the epitaxial quality and physical properties. Chen and his collaborators proposed and systematically investigated the effect from the surface step terrace height and surface terminations on the film growth dynamics. For instance, MgO has types of surface terminations along the [001] direction but has the same atomic structures. The two surface terminations are displaced a half unit-cell along the [100] MgO direction with respect to each other. Each termination has a half unit-cell step height difference on the (001) MgO surface. Recent research indicates that the growth of the initial layer of BSTO film on the (001) MgO surface is a TiO_2 monolayer [46]. Thus, the BSTO thin films on a (001) MgO substrate form two types of epitaxial domains that have a half unit-cell shift along the *c*-axis direction. The steps with different heights will result in the formation of different domains (antidomains) in the films. Figure 7c is a TEM image showing an antidomain boundary of a BSTO thin film formed on a (001) MgO and Fig. 7d is a HRTEM image detailing the antidomain boundary directly formed from the surface step terrace. This can be well-explained by the schematic in Fig. 8a showing the detailed surface structures of a MgO surface. When BSTO thin films grow on a (001) MgO substrate that normally consists of steps with a height of half a unit-cell [$\frac{1}{2}a_{MgO}$ (step 2 in Fig. 7d)] or unit-cell height [a_{MgO} (step 1 in Fig. 7d)], the BSTO crystal grown on terrace II will be displaced by $\frac{1}{2}a_{BSTO}$ along the [001] MgO growth direction with respect to the structure on terrace III. Thus, a conservative antiphase boundary (with the displacement vector parallel to the boundary plane) that is parallel to the growth direction is formed between these two steps. A half unit-cell height shift between these two domains can be clearly revealed in the image. Similarly, the terrace structures of the substrate will also affect the microstructure of the thin films. As stated above, the first monolayer of the BSTO thin films on the MgO substrate was identified as the TiO_2 monolayer. It is reasonable to assume that during the growth of the first TiO_2 monolayer, which is the adjacent layer to the substrate step, is the Ti–O atomic chain. If the substrate surface terrace width is equal to n unit cells of the BSTO films and the first adjacent atom is Ti, the atom at the end of the terrace should be O. Hereafter, the next adjacent atom from the second layer of the lower (half a unit-cell different) step terrace will be an O atom again which will result in an O–O atomic chain at the domain boundary; and so on. Similarly, when a terrace width is equal to $\left(n+\frac{1}{2}\right)$ BSTO unit cells and is of a single MgO step height, the initial row and the last row will be Ti–O atomic chains. Accordingly, in the as-grown BSTO structure, the first and the last crystal planes that are parallel to both growth direction and step would be the TiO_2 planes. The TiO_2 planes of two adjacent terraces will adhere at the last or topmost TiO_2 plane. In other words, the BSTO grown on the terrace with a width of an odd number of a_{MgO} will be displaced by a_{BSTO} with respect to that on the

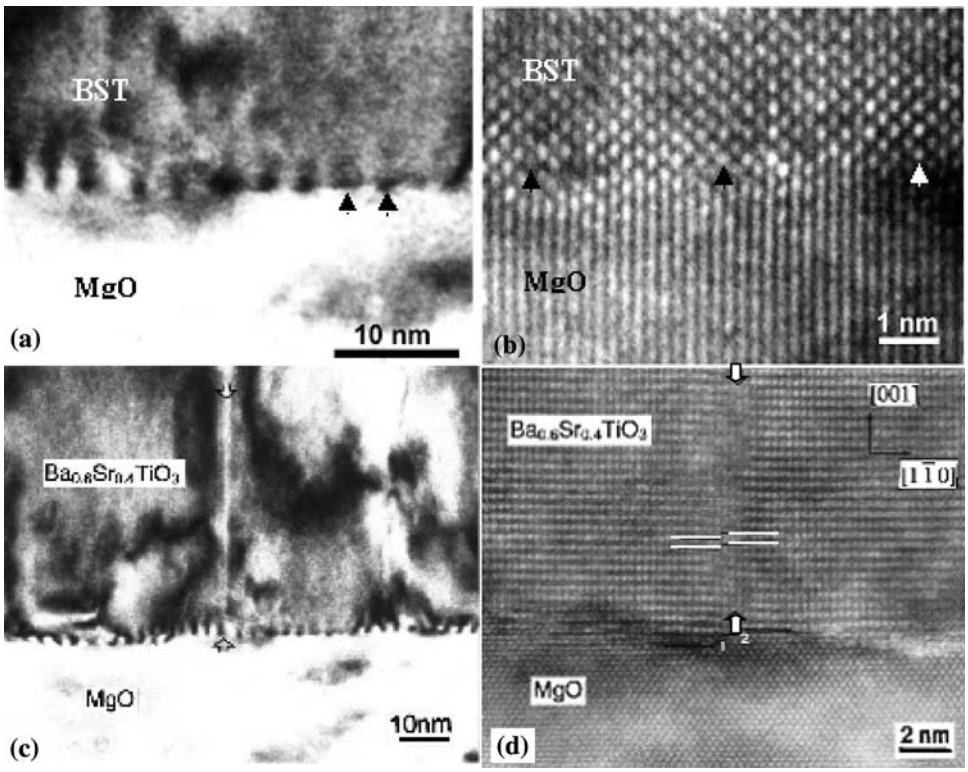

Fig. 7 **a** Cross-sectional TEM image of $Ba_{0.6}Sr_{0.4}TiO_3$/MgO. **b** High-resolution TEM image showing the edge dislocations were formed periodically along the interface. **c** Dark-field high-resolution TEM image of an antiphase domain boundary was formed in the epitaxial films. **d** HRTEM image of the $Ba_{0.6}Sr_{0.4}TiO_3$/MgO interface showing an antiphase domain boundary was generated from a substrate surface step terrace [47]

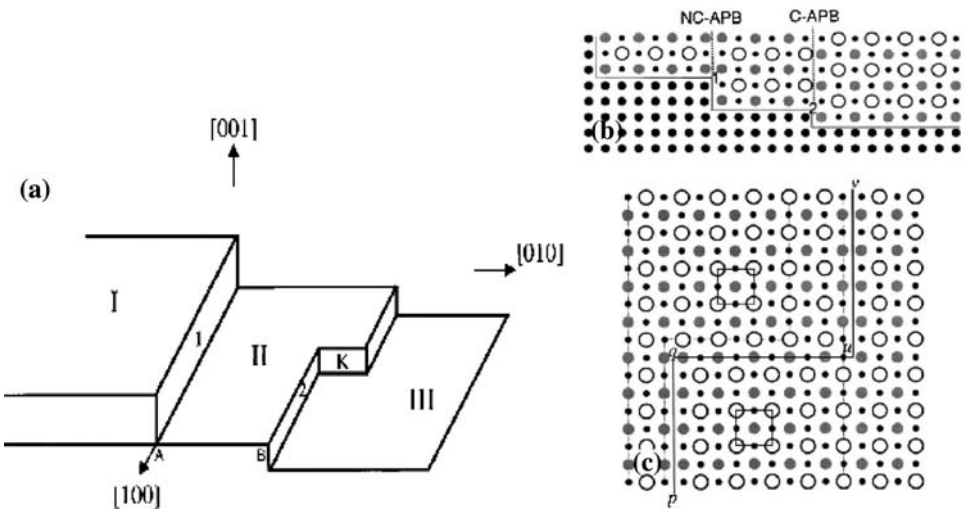

Fig. 8 **a** Schematic illustration of the (001) MgO substrate surface showing steps, terraces, and kinks. **b** The [100]MgO projection of the $Ba_{0.6}Sr_{0.4}TiO_3$/MgO interface. **c** The [001] projection of the $Ba_{0.6}Sr_{0.4}TiO_3$ showing kinks induced antiphase domain boundaries [47]

adjacent terraces along the direction that is perpendicular to the steps. A step one half unit-cell high in the MgO substrate forces the cubic structure of BSTO to slightly adjust itself to compensate for the half unit-cell displacement. A nonconservative antiphase boundary (with the displacement vector perpendicular to the boundary plane) that is parallel to the growth direction and the step, subsequently forms between the structures grown on the adjacent terraces (NC-APB in Fig. 8b). Within a thin film grown on a terrace with a width of an even number of a_{MgO}, a nonconservative antiphase boundary will not be formed in the BSTO structures grown on the adjacent terraces. These results indicate that the substrate surface can strongly affect the microstructures of as-grown films. These growth models can be extended to all other perovskite thin films on MgO surfaces and other materials. Also, the strong effects from surface step terraces have recently been observed from miscut substrates, as described below.

In fact, the antiphase domain structures in the highly epitaxial ferroelectric thin films have been observed on various systems. Kwak et al. [46] experimentally observed domain patterns on epitaxial $PbTiO_3$ heterostructures. For $PbTiO_3/KTaO_3$ heterostructure, periodic domain pattern was observed in the overlayer; in $PbTiO_3/SrTiO_3$ system,

the film exists as a single *c*-domain due to the excellent lattice match; in $PbTiO_3$/MgO system which has a poor lattice match, it appeared to find the energy minimum by locking into domains of two-dimensional superlattices with the greatest atomic coincidences. The domain patterns were found to be strongly related to the film thickness and measuring temperature as well. By using linear-elasticity theory for the substrate and a Landau–Ginzburg–Devonshire-type phenomenological theory for the ferroelectric film, they also developed a theoretical model to explain the domain patterns as a "strain accommodating" mechanism.

Speck and Pompe et al. [43–45] performed a detailed investigation on possible mechanisms for strain relaxation and domain stability in ferroelectric thin films. Temperature dependent stability maps have been developed that predict the stable domain structure that forms during the PE to FE transition. The stability maps incorporated the role of the following parameters: (i) substrate lattice parameter, (ii) differential thermal expansion characteristics between the film and substrate, (iii) cooling rate, and (iv) depolarizing fields and electrode geometry. Furthermore, the role of dislocation stabilization of domain patterns has been discussed. The models are applicable to tetragonal thin film ferroelectrics grown epitaxially on (001) cubic single crystal substrates. It showed that misfit dislocations generated during growth screen the majority of the lattice mismatch with the substrate. Thus, the variety of domain patterns that develop during the Curie transition depend on processing parameters and can be successfully explained by applying the temperature dependent coherent domain stability map theoretically developed.

Another model for the formation of domain and dislocation was proposed by Misirlioglu et al. [51] based on the observations on PLD grown epitaxial (001) ferroelectric $PbZr_{0.2}Ti_{0.8}O_3$ films on (001) $SrTiO_3$ substrates. TEM revealed that the films were predominantly *c*-oriented with embedded a1- and a2-oriented domains lying on {101} planes. Arrays of edge-type misfit dislocations were observed at substrate/film interfaces and there were extraordinarily high densities ($\sim 10^{10}$ cm^{-2}) of threading dislocations in the films. The authors suggested that: misfit dislocations occur at the growth temperature and may be forced away from the interface to form threading dislocations during island coalescence, domains with different orientations may form beside the dominated-oriented domain upon cooling through the Curie temperature to ameliorate the self-strain of the transformation, stresses caused by expansion coefficient difference may lead to some redistribution of the embedded domains and misfit dislocations.

Considering the partial relaxation of epitaxial coherency strains, a strain gradient along the growth orientation was proposed, and accordingly, a three-dimensional domain structure was observed by Towner et al. [26]. Based on the results from a serial sectioning technique, it was found that the domain structure varied sharply through the thickness for the $BaTiO_3$ thin films on MgO substrates. It is primarily *a*-oriented near the substrate and increasingly *c*-oriented away from this interface. The refractive index also varied through the film thickness. Gradients in the strain can explain the relaxor-like behavior often observed in ferroelectric thin films. In 2005, Catalan et al. [27] used X-ray analysis to study the ferroelectric thin layers of $Ba_{1/2}Sr_{1/2}TiO_3$ with different thicknesses. The data also revealed the presence of strain gradients across the films. A functional form for the internal strain profile was proposed and used to calculate the influence of strain gradient on the degradation of the ferroelectric properties of films with decreasing thickness. The results are in excellent agreement with the experimental data. They show that strain relaxation can lead to smooth, continuous gradients across hundreds of nanometers. Similarly, inhomogeneous strain along the growth direction was observed in a 100 nm thick $BaTiO_3$ film deposited on platinized Si substrate [60].

Interface strain effects on dielectric properties

Various methods have been tried to tune the strain in the highly epitaxial ferroelectric thin film for optimizing the dielectric properties. One of the most common methods is to adapt different substrates for the film growth. Many researches have been carried out to understand the dielectric and piezoelectric response of ferroelectric thin films on various substrates [7–11]. By investigating 100-nm-thick epitaxial $0.9[Pb(Mg_{1/3}Nb_{2/3})O_3]$–$0.1[PbTiO_3]$ (PMN–PT) thin films on (001)$LaAlO_3$ (LAO), (La,Sr)(Al, Ta)O_3 (LSAT), $SrTiO_3$ (STO), and MgO substrates, the effects of substrates on the electrical and electromechanical properties were systematically explored by Nagarajan et al. [7]. They observed a decrease in the temperature of dielectric maximum (T_m) together with an increase in the dielectric constant and the longitudinal piezomodulus when decreasing in-plane epitaxial compressive stresses in the films, whereas, the films on MgO substrates, which exhibit tensile stress, exhibit the highest dielectric constant and piezomodulus with the T_m dropping to below room temperature. Chang et al. [8] investigated epitaxial BST thin films on (100) MgO and LAO substrates and found that strain is closely related to the dielectric properties as limiting the ability to obtain both high tuning and high dielectric Q in epitaxial BST thin films. Dielectric properties were theoretically analyzed as a function of electric field and strain. Hyun's data indicated the tensile strain along the applied electric field in the parallel plate capacitor enhances the dielectric constant and the tunability, while the compressive strain decreases both dielectric

parameters [9]. The results are consistent with the hardening of the soft mode phonon due to the compressive strain.

The thickness of the film has been considered to be another factor to effectively tune the strain, considering the thickness dependence of stress relaxation by misfit dislocation formation at the deposition temperature. For epitaxial films of relaxor ferroelectric PMN-PT, a change of the film thickness from 100 to 400 nm results in nearly an order-of-magnitude increase in the dielectric constant and the piezoresponse of the film, as well as a decrease in the phase transition temperature from ~250 to ~60 °C [16]. Systematical studies were performed on the heteroepitaxial $Ba_{0.6}Sr_{0.4}TiO_3$ thin films grown on $0.29(LaAlO_3)$:0.35 (Sr_2TaAlO_6) substrates using pulsed-laser deposition [17]. X-ray characterization revealed compressive in-plane stresses in the thinnest films, which were relaxed in a continuous fashion with increasing thickness. A theoretical treatment of the misfit strain was in good agreement with the measured out-of-plane lattice parameter. The low-frequency dielectric constant was measured to be significantly less than the bulk value and found to decrease rapidly for films less than 100 nm. A thermodynamic model was developed to understand the reduction in dielectric constant. By observing the microstructure using plan-view and cross-section transmission electron microscopy, we identified local strain associated with a threading dislocation density on the order of 10^{11} cm^{-2} as a possible mechanism for dielectric degradation in these films.

A number of efforts have been focused on the studies of the strain effects on the dielectric properties on various substrates and different film thicknesses, the results imply a strong correlation between strain and dielectric properties of ferroelectric thin films. However, the effects on the dielectric properties can not be distinguished from strain and other factors such as crystallinity since the current data are the strain from various substrates and film thicknesses. Specifically, the difference in crystalline quality among the films on different substrates and different thicknesses is hard to control, especially when using different substrates. For example, the full width at half maximum (FWHM) of XRD rocking curve for the BST-0.4 films on MgO are 5 time larger than those on LAO even at the exact same deposition condition, indicating that the change of the dielectric properties (as much as near 20% change) is also associated to the crystallinity of the films [61].

Park proposed a method to minimize the quality difference between samples by inserting a very thin BST-x (x = 0.1– 0.7) interlayer between the MgO substrate and the main layer of BST-0.4. The stress states, i.e., the lattice distortion ratio (D = in-plane lattice constant/out-of-plane lattice constant) of the BST-0.4 films have been successfully controlled by varying the chemical composition of the interlayers. It has been found that small variations of D value can result in significantly large changes of dielectric properties. A BST-0.4 film under small tensile stress, which has a D value of 1.0023, shows the largest dielectric permittivity and tunability [62].

All of the previous researches, both on various substrates and different film thicknesses as well as the buffered epitaxy, of the strain effects on the ferroelectric epitaxy and physical properties discussed above were performed on cubic substrates. These researches can not exclude other factor effects on the physical properties and epitaxial nature. To fully understand the strain effects on the highly epitaxial ferroelectric thin films, Lin et al. [63, 64] paved a new way to study the strain effects and strain distributions by studying the epitaxial ferroelectric PSTO thin films on non-cubic substrates. They selected an orthorhombic substrate ($NdGaO_3$), which has different in-plane lattice parameters, inducing anisotropic in-plane strains in the high quality epitaxial growth of PST thin films on $NdGaO_3$ substrates. The in-plane strains, determined by high-resolution XRD, were 485 ppm along PST[100] and 26 ppm along PST[010], respectively. By using co-planar stripline structure along these two in-plane directions, obvious anisotropy in dielectric properties was observed, i.e., about 15% difference in tunability at a surface field of 50 kV/cm and 20% difference in zero-field dielectric constant. The comparisons of the strain as well as the dielectric properties were performed on two in-plane directions of the same sample, which will exclude the impact from the variation of sample qualities. Further studies indicated that the post deposition cooling rate plays an important role in determining both the structural and the dielectric properties of the PST films on (110) NGO substrate. Both slowly cooled and fast cooled films have shown anisotropic dielectric properties. The highest dielectric values are obtained for the slowly cooled sample (ε_0 = 4220, tunability = 59% at 50 kV/cm). Compared to the fast cooled sample, the slow cooled sample has shown an even more obvious anisotropy in dielectric properties, i.e., about a 20% difference in tunability at 50 kV/cm and a 48% difference in ε_0. The reasons are from the different final strain status of the fast cooled and slow cooled sample, which may be caused by the strain relaxation during cooling process and a possible variation in oxygen stoichiometry. Figure 9a–f are the high-resolution X-ray diffraction reciprocal space maps from the slow cooled (Fig. 9a–c) and fast cooled (Fig. 9d–f) samples, respectively, indicating anisotropic in-plane strains for both samples and different strain status between the two samples. Figure 9g shows dielectric constant versus the surface electric field along the x and y directions for both samples. It should be noted that the samples presented in this work show very high epitaxial quality with the FWHM of rocking curves less than 0.08°,

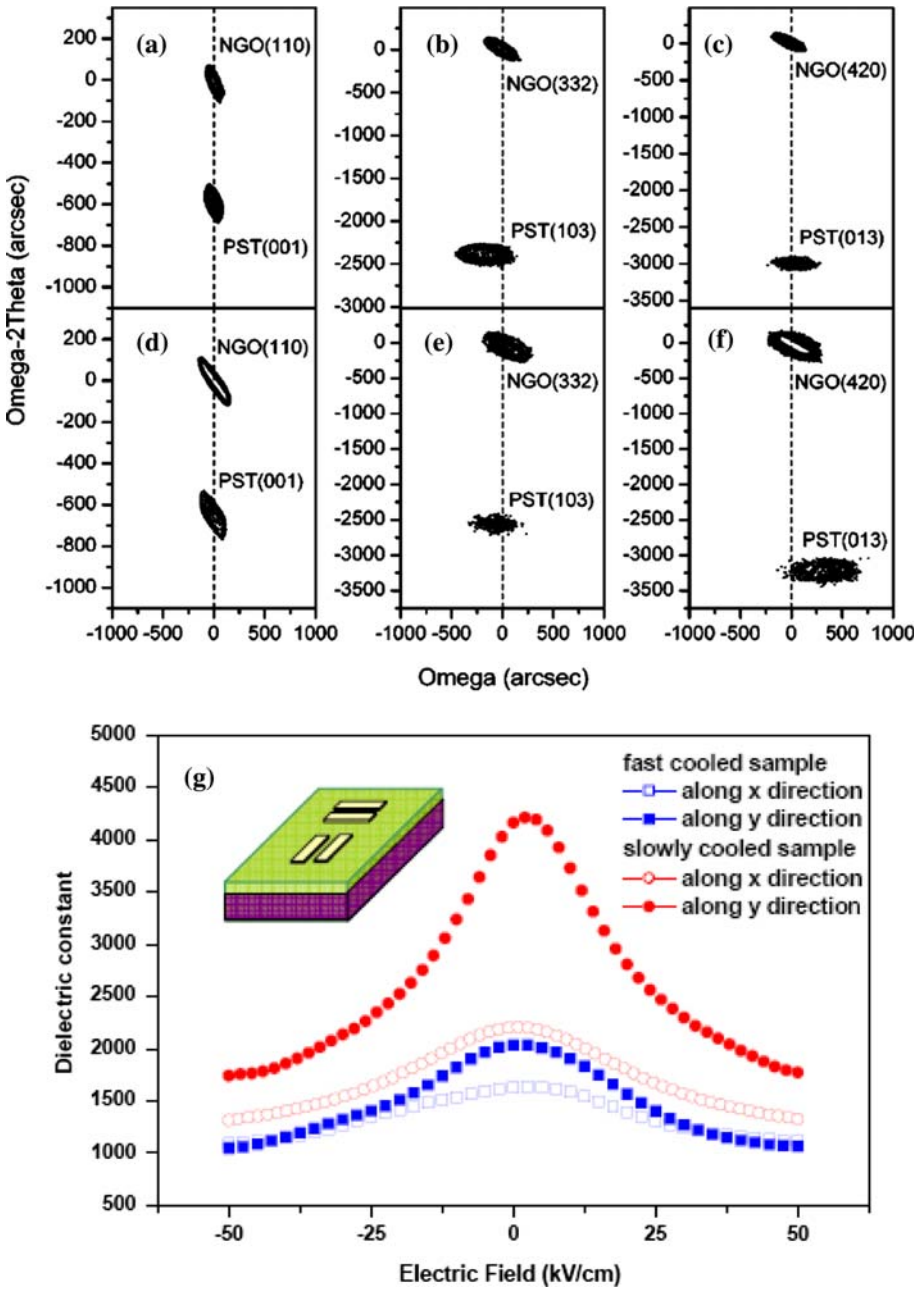

Fig. 9 Reciprocal space maps around **a** PST (001) and NGO (110); **b** PST (103) and NGO (332); **c** PST (013) and NGO (420) for the slowly cooled sample; and **d** PST (001) and NGO (110); **e** PST (103) and NGO (332); **f** PST (013) and NGO (420) for the fast cooled sample. **g** The dielectric constants of slowly cooled and fast cooled samples at 1 MHz and room temperature as a function of the applied electric fields. The inset of **g** shows the schematic of the pattern for the dielectric measurements [63, 64]

which again has ensured minimal impact from dislocations and non-perfect crystallinity. Soon after the experimental data was published, Zembilgotov et al. [65] developed "misfit strain-temperature" phase diagrams for ferroelectric films on orthorhombic substrates. A nonlinear thermodynamic theory is used to predict the equilibrium polarization states and dielectric properties of ferroelectric thin films grown on these substrates which induce anisotropic strains in the film plane. It is shown that the in-plane strain anisotropy may lead to the appearance of new phases which do not form in films grown on cubic substrates. With this theory, the strain-induced dielectric anisotropy in the film plane was calculated and found to be in reasonable agreement with the experimental data from Lin et al.

A great breakthrough was achieved in 2004, when biaxial strain was used to markedly enhance the ferroelectric properties of thin films. $BaTiO_3$ and $SrTiO_3$ thin films were grown fully coherently on single-crystal $GdScO_3$ and $DyScO_3$ substrates. For the $BaTiO_3/GdScO_3$ and $BaTiO_3/DyScO_3$ systems, the strain can result in a ferroelectric transition temperature nearly 500 °C higher and a remanent polarization at least 250% higher than bulk $BaTiO_3$ single crystals [66]. More significantly, room-temperature ferroelectricity was produced in $SrTiO_3$, a

material that is not normally ferroelectric at any temperature. A high dielectric constant of nearly 7,000 at 10 GHz and room temperature in the $SrTiO_3/DyScO_3$ films and sharp dependence on electric field were observed, as shown in Fig. 10 [67]. This is a remarkable success in the field of strain engineering for ferroelectric thin films making these strained films with excellent ferroelectric properties very promising for device applications.

Besides the single layer structures, multilayers and superlattices were also investigated. The interface structure, strain configuration, and strain relaxation in such systems are different from those in single layer systems. Interfacial coupling should be considered when the thickness of each layer is small enough.

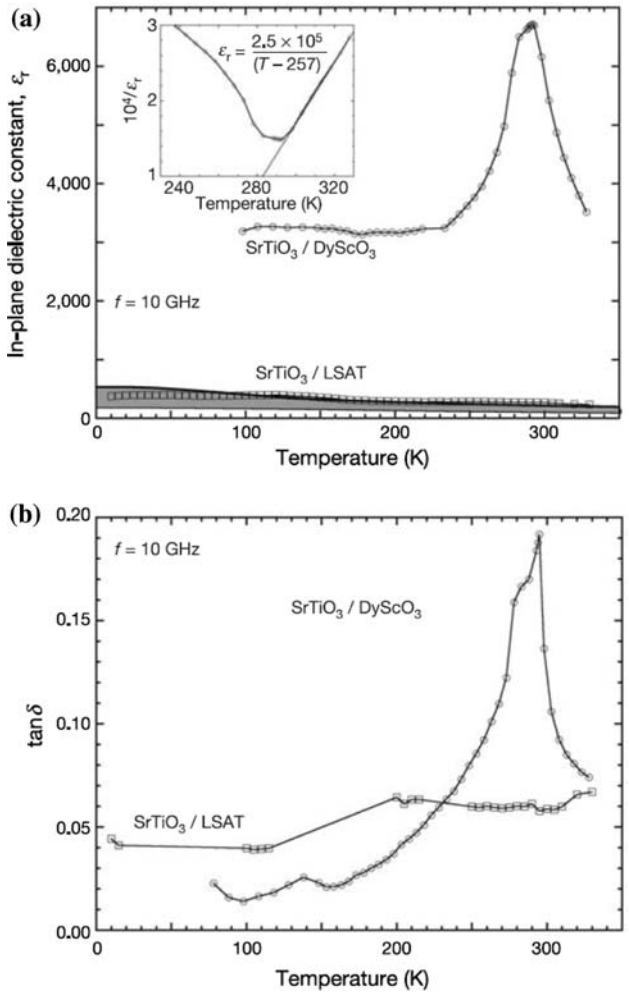

Fig. 10 From Ref. [67]. **a** In-plane dielectric constant (ε_r) and **b** dielectric loss (tan δ) in 500 Å-thick $SrTiO_3$/(110) $DyScO_3$ and $SrTiO_3$/(100) LSAT epitaxial films as a measurement frequency of 10 GHz. These films are under biaxial tensile and compressive strain, respectively. The peak in ε_r of about 7,000 and the simultaneous peak in tan δ indicate that the T_c of $SrTiO_3$ under biaxial tension of 0.008 is about 293 K. The inset in **a** shows a Curie–Weiss fit to $1/\varepsilon_r$. Owing to systemic errors involved in the measurement and calculation of the in-plane dielectric constant, the vertical scale in a may be off by as much as 10%. The shaded region in **a** corresponds to the expected value of the in-plane ε_r for a SrTiO3 film commensurately strained to LSAT (strain = −0.009), based on thermodynamic analysis and the range of relevant reported property coefficients for $SrTiO_3$ [75, 76]

It is interesting to note that Lee et al. reported their pioneered work in *Nature* of the fabrication and investigation of the superlattices consisting of $BaTiO_3$, $SrTiO_3$, and $CaTiO_3$ on $SrRuO_3$ layers [68]. By preserving full strain and combining heterointerfacial couplings, they observed a 50% overall enhancement of the superlattice global polarization with respect to similarly grown pure $BaTiO_3$, despite the fact that half the layers in the superlattice are nominally non-ferroelectric, as shown in Fig. 11. Furthermore, Tenne et al. reported on *Science* that one-unit-cell-thick $BaTiO_3$ layers in $BaTiO_3/SrTiO_3$ superlattices are not only strongly ferroelectric but also polarize the quantum paraelectric $SrTiO_3$ layers adjacent to them. The mechanical boundary condition imposed by the $SrTiO_3$ substrate leads to strain in the $BaTiO_3$ layers and thus to enhanced ferroelectricity [69]. The interplay between the electrical and mechanical boundary conditions enables the tuning of T_c by nearly 500 K. To understand the nature of the superior improvement of ferroelectricity in superlattices, several models and experimental techniques have been used to find a proper explanation. For $SrTiO_3$ layers within the superlattices, ultraviolet Raman measurements and phase field simulations in Refs. [69] and [70] showed that it only exhibited induced polarization, while in Refs. [71] and [72] orthorhombic distortion was observed. Li et al. [73] provided a consistent explanation of different conclusions in the literature with regard to the ferroelectricity of $SrTiO_3$ layers in $BaTiO_3/SrTiO_3$ superlattices. They theoretically studied the phase transitions, domain morphologies, and polarizations in $BaTiO_3/SrTiO_3$ superlattices grown on $SrTiO_3$ substrates using the phase field approach. It was found that the coherency between a superlattice film and the substrate has a dramatic effect on the ferroelectricity of $SrTiO_3$ layers within the superlattice. With an incoherent interface, the $SrTiO_3$ layer is an orthorhombic ferroelectric while with a coherent interface it exhibits only an induced polarization from the adjacent $BaTiO_3$ layers.

More recently, Weiss et al. reported that a high tunability, that is temperature insensitive, has been achieved in compositionally graded ferroelectric Barium Strontium Titanate ($Ba_{1-x}Sr_xTiO_3$ or ml-BST) multilayer heterostructures [40, 74]. Both experimental results and theoretical modeling demonstrate that stress plays a key role in affecting the dielectric properties. Analysis of compositionally graded ml-BST multilayers reveals that, at room temperature, the ml-BST heterostructure on Pt buffered Si has a small-signal dielectric permittivity of 360 with a dissipation factor of 0.012, a dielectric tunability of 65% at 444 kV/cm and that its dielectric loss can be improved to tan $\delta = 0.008$ in

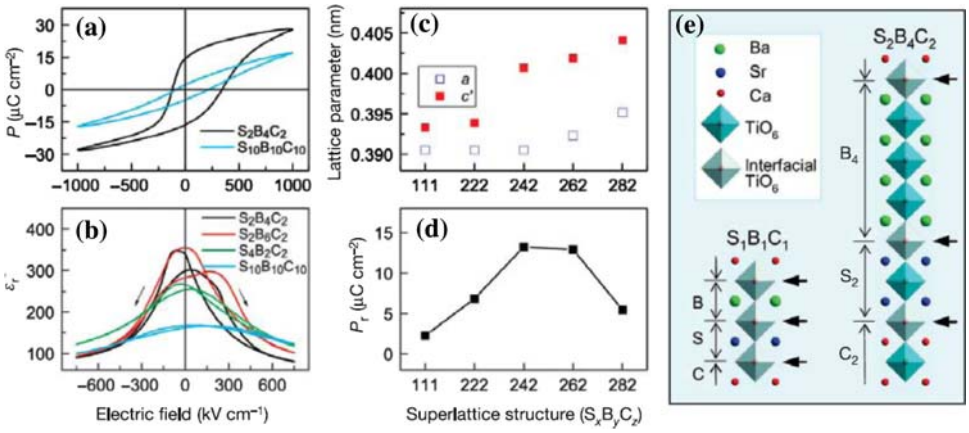

Fig. 11 From Ref. [68]. Polarization enhancement, changes in asymmetry, and evolution of strain in TCS structures. **a** P(E) curves of $S_2B_4C_2$ ($P_r \approx 16.5$ μC cm^{-2}) and $S_{10}B_{10}C_{10}$ ($P_r \approx 3.5$ μC cm^{-2}) at 1000 kV cm^{-1} (Note that this electric field is higher than that applied to measure the polarization of the $BaTiO_3$ film, whose polarization is near saturation at 400 kV cm^{-1}, whereas the $S_2B_4C_2$ requires a higher electric field ($\sim$700 kV cm^{-1})). **b** ε(E) curves of $S_2B_4C_2$ (*black line*), $S_2B_6C_2$ (*red line*), $S_4B_2C_2$ (*green line*) and $S_{10}B_{10}C_{10}$ (*light blue line*) showing differing degrees of asymmetry. **c** In-plane (*open squares*) and out-of-plane (*filled squares*) lattice parameters of various superlattices. c′ corresponds to the supercell c divided by the number of constituent perovskites in a supercell. **d** P_r values from $E = \pm 750$ kV cm^{-1} loops. The partially relaxed $S_2B_8C_2$ structure was measured with $E = \pm 650$ kV cm^{-1} because of its lower breakdown strength. **e** Diagrams of supercells showing the different local environments possible for the TiO6-octahedra (bound by the same or different A-site cations). Heterointerfacial TiO_6 octahedra are shaded in *gray* and indicated by *solid black arrows*

MgO-doped ml-BST heterostructures. The results indicate that such a multilayered structure can significantly enhance the dielectric properties, both dielectric tunability and dielectric loss, of ferroelectric thin films for tunable microwave device applications.

Summary

The physical properties of highly epitaxial thin films are strongly dependent upon the interface atomic structures such as lattice misfit, surface step terraces, and substrate surface terminations. The interface strain energy from lattice misfit is usually released by forming the edge dislocations at the entire interface between the film and substrate. However, the strain energy from the mismatch between the film unit-cell arrangement and substrate surface step terrace dimension can not be released by forming edge dislocations, which will result in the microstructure deformations. Furthermore, the surface step terrace height will result in the formation of the antiphase domain structures in the highly epitaxial ferroelectric thin films. Systematical studies on the relationship between the growth dynamics, interface effects, and dielectric properties are not only scientific necessary but also technological important for new concept novel device fabrications. Controlling the interface structures with optimizing physical properties will pave the new way for designing and fabricating interface engineered metamaterials with desired properties. The interface engineered metamaterials may become the building blocks for modern electronic device developments and the genuine for the physical phenomena discovery in ferroelectric and multiferroic advanced materials.

Acknowledgements The authors gratefully acknowledge the support of the National Science Foundation, the Department of Energy, the Army Research Office, the Texas Higher Education ARP Program, and the State of Texas through the TcSUH at University of Houston.

References

1. Joshi PC, Cole MW (2000) Appl Phys Lett 77:289
2. Chen CL, Feng HH, Zhang Z, Brazdeikis A, Huang ZJ, Chu WK, Chu CW, Miranda FA, Van Keuls FW, Romanofsky RR, Liou Y (1999) Appl Phys Lett 75:412
3. Kotechi DE (1997) Integr Ferroelectr 16:1
4. Dalberth MJ, Stauber RE, Price JC, Roger CT, Galt D (1998) Appl Phys Lett 72:507
5. Jia QX, Findikoglu AT, Reagor D, Lu P (1998) Appl Phys Lett 73:897
6. Schwarzkopf J, Fornari R (2006) Prog Cryst Growth Charact Mater 52:159
7. Nagarajan V, Alpay SP, Ganpule CS, Nagaraj B, Aggarwal B, Williams ED, Roytburd AL, Ramesh R (2000) Appl Phys Lett 77:438
8. Chang W, Gilmore CM, Kim WJ, Pond JM, Kirchoefer SW, Qadri SB, Chirsey DB, Horwitz JS (2000) J Appl Phys 87:3044
9. Hyun S, Char K (2001) Appl Phys Lett 79:254
10. Trithaveesak O, Schubert J, Ch Buchal (2005) J Appl Phys 98:114101
11. Chen YB, Sun HB, Katz MB, Pan XQ, Choi KJ, Jang HW, Eom CB (2007) Appl Phys Lett 91:252906

12. Chen CL, Shen J, Chen SY, Luo GP, Chu CW, Miranda FA, Van Keuls FW, Jiang JC, Meletis EI, Chang H (2001) Appl Phys Lett 78:652
13. Liu SW, Weaver J, Lin Y, Donner W, Chen X, Chen CL, Jiang JC, Meletis EI, Bhalla AS (2004) Appl Phys Lett 85:3202
14. Yano Y, Iijima K, Daitoh Y, Terashima T, Bando Y, Watanabe Y, Kasatani H, Terauchi H (1994) J Appl Phys 76:7833
15. Li H, Roytburd AL, Alpay SP, Tran TD, Salamanca-Riba L, Ramesh R (2001) Appl Phys Lett 78:2354
16. Nagarajan V, Ganpule CS, Nagaraj B, Aggarwal S, Alpay SP, Roytburd AL, Williams ED, Ramesh R (1999) Appl Phys Lett 75:4183
17. Canedy CL, Li H, Alpay SP, Salamanca-Riba L, Roytburd AL, Ramesh R (2000) Appl Phys Lett 77:1695
18. Ellerkmann U, Liedtke R, Boettger U, Waser R (2004) Appl Phys Lett 85:4708
19. Hofer C, Halder S, Waser R (2006) Ferroelectrics 332:153
20. Katayama I, Shimosato H, Ashida M, Kawayama I, Tonouchi M, Itoh T (2008) J Lumin 128:998
21. Alguero M, Calzada ML, Martin MJ, Pardo L (2002) J Phys Chem Solids 63:471
22. Iakovlev S, Solterbeck CH, Es-Souni M (2002) Appl Phys Lett 81:1854
23. Jing Y, Luo J (2005) Sens Actuators A 121:103
24. Sumi K, Qiu H, Kamei H, Moriya S, Murai M, Shimada M, Nishiwaki T, Takei K, Miyashita S, Hashimoto M (1998) Thin Solid Films 330:183
25. Wu L, Wu J (2007) J Cryst Growth 308:424
26. Towner DJ, Lansford TJ, Wessels BW (2004) J Electroceram 13:89
27. Catalan G, Noheda B, McAneney J, Sinnamon LJ, Gregg JM (2005) Phys Rev B 72:020102R
28. Devonshire AF (1949) Philos lag 40:1040
29. Forsbergh PW (1954) Phys Rev 93:686
30. Haun MJ, Furman E, Jang SJ, McKinstry HA, Cross LE (1987) J Appl Phys 62:3331
31. Rossetti GA, Udayakumar KR, Haun MJ, Cross LE (1990) J Am Ceram Soc 73:3334
32. Kushida K, Takeuchi H (1990) Ferroelectrics 108:3
33. Kushida K, Takeuchi H (1991) IEEE Trans, Ultrason Ferroelectr Freq Control (Special Issue on Ferroelectric Thin Films)
34. Rossetti GA, Cross LE, Kushida K (1991) Appl Phys Lett 59:2524
35. Pertsev NA, Zembilgotov AG, Tagantsev AK (1998) Phys Rev Lett 80:1988
36. Pertsev NA, Zembilgotov AG, Hoffmann S, Waser R, Tagantsev AK (1999) J Appl Phys 85:1698
37. Streiffer SK, Basceri C, Parker CB, Lash SE, Kingon AI (1999) J Appl Phys 86:4565
38. Chen JH, Jia CL, Urban K, Chen CL (2002) Appl Phys Lett 81:1291
39. Ban ZG, Alpay SP (2002) J Appl Phys 91:9288
40. Okatan MB, Cole MW, Alpay SP (2008) J Appl Phys 104: 104107
41. Jiang JC, Meletis EI, Yuan Z, Chen CL (2007) Appl Phys Lett 90:051904
42. Jiang JC, He J, Meletis EI, Liu J, Yuan Z, Chen CL, Dong C (2008) J Nano Res 3:59
43. Pompe W, Gong X, Suo Z, Speck JS (1993) J Appl Phys 74:6012
44. Speck JS, Pompe W (1994) J Appl Phys 76:466
45. Speck JS, Seifert A, Pompe W, Ramesh R (1994) J Appl Phys 76:477
46. Kwak BS, Erbil A, Buda JD, Chisholm MF, Boatner LA, Wilkens BJ (1994) Phys Rev B 49:14865
47. Jiang JC, Lin Y, Chen CL, Chu CW, Meletis EI (2002) J Appl Phys 91:3188
48. Gao HJ, Chen CL, Rafferty B, Pennycook SJ, Luo GP, Chu CW (1999) Appl Phys Lett 75:2542
49. Liu SW, Weaver J, Donner W, Yuan Z, Chen CL, Jiang JC, Meletis EI, Chang W, Kirchoefer SW, Horwitz J, Bhalla A (2005) Appl Phys Lett 87:142905
50. Liu SW, Chakhalian J, Xiao X, Chen CL (2007) Appl Phys Lett 90:042901
51. Misirlioglu IB, Vasiliev AL, Alpay SP, Aindow M, Ramesh R (2006) J Mater Sci 4:697. doi:10.1007/s10853-006-6488-9
52. Alpay SP, Misirlioglu IB, Nagarajan V, Ramesh R (2004) Appl Phys Lett 85:2044
53. Zheng Y, Wang B, Woo CH (2007) J Mech Phys Soli 55:1661
54. Tian HF, Yu HC, Zhu XH, Wang YG, Zheng DN, Yang HX, Li JQ (2005) Phys Rev B 71:115419
55. Li YL, Hu SY, Choudhury S, Baskes MI, Saxena A, Lookman T, Jia QX, Schlom DG, Chen LQ (2008) J Appl Phys 104:104110
56. Nagarajan V, Jia CL, Kohlsteda H, Waser R, Misirlioglu IB, Alpay SP, Ramesh R (2005) Appl Phys Lett 86:192910
57. Henrich VE, Cox PA (1994) The surface science of metal oxides. Cambridge University Press, Cambridge
58. Jiang JC, Chen CL, Lin Y, Horwitz J, Jacobson AJ, Meletis EI, Phil Mag Lett (in press)
59. Chen CL, Lin Y, Yuan Z, Li Y, Horwitz J, Jiang JC, Meletis EI, Jacobson AJ, Nature Mat (submitted)
60. Brahim D, Emmanuel D, Julie G (2007) Appl Phys Lett 90:022908
61. Lee JS, Lin Y (2003) MRS Fall Meeting, Boston, MA, Dec 1–4
62. Park BH, Peterson EJ, Jia QX, Lee J, Si W, Xi XX (2001) Appl Phys Lett 78:533
63. Lin Y, Chen X, Liu SW, Chen CL, Lee JS, Li Y, Jia QX, Bhalla A (2004) Appl Phys Lett 84:577
64. Lin Y, Chen X, Liu SW, Chen CL, Lee JS, Li Y, Jia QX, Bhalla A (2005) Appl Phys Lett 86:142902
65. Zembilgotov AG, Pertsev NA, Böttger U, Waser R (2005) Appl Phys Lett 86:052903
66. Choi KJ, Biegalski M, Li YL, Sharan A, Schubert J, Uecker R, Reiche P, Chen YB, Pan XQ, Gopalan V, Chen LQ, Schlom DG, Eom CB (2004) Science 306:1005
67. Haeni JH, Irvin P, Chang W, Uecker R, Reiche P, Li YL, Choudhury S, Tian W, Hawley ME, Craigo B, Tagantsev AK, Pan XQ, Streiffer SK, Chen LQ, Kirchoefer SW, Levy J, Schlom DG (2004) Nature 430:758
68. Lee HN, Christen HM, Chisholm MF, Rouleau CM, Lowndes DH (2005) Nature 433:395
69. Tenne DA, Bruchhausen A, Lanzillotti-Kimura ND, Fainstein A, Katiyar RS, Cantarero A, Soukiassian A, Vaithyanathan V, Haeni JH, Tian W, Schlom DG, Choi KJ, Kim DM, Eom CB, Sun HP, Pan XQ, Li YL, Chen LQ, Jia QX, Nakhmanson SM, Rabe KM, Xi XX (2006) Science 313:1614
70. Li YL, Hu SY, Tenne D, Soukiassian A, Schlom DG, Xi XX, Choi KJ, Eom CB, Saxena A, Lookman T, Jia QX, Chen LQ (2007) Appl Phys Lett 91:112914
71. Rios S, Ruediger A, Jiang AQ, Scott JF, Lu HB, Chen ZH (2003) J Phys: Condens Mater 15:305
72. Jiang AQ, Scott JF, Lu HB, Chen ZH (2003) J Appl Phys 93:1180
73. Li YL, Hu SY, Tenne D, Soukiassian A, Schlom DG, Chen LQ, Xi XX, Choi KJ, Eom CB, Saxena A, Lookman T, Jia QX (2007) Appl Phys Lett 91:252904
74. Liu M, Collins G, Silva E, Liu J, Chen CL, Jiang JC, Meletis EI, Cole MW, Nat Mater (submitted)
75. Hellwege K-H, Hellwege AM (eds) (1981) Landolt-Börnstein: numerical data and functional relationships in science and technology new series, Group III, vol 16a. Springer, Berlin, p 59
76. Hellwege K-H, Hellwege AM (eds) (1979) Landolt-Börnstein: numerical data and functional relationships in science and technology new series, Group III, vol 11. Springer, Berlin, p 418